Landau expansion parameters and the *O-T* phase transition of a $0.64Pb(Mg_{1/3}Nb_{2/3})O_3$-$0.36PbTiO_3$ single crystal

Hangbo Zhang,[1] Xiaoyan Lu,[1,*] Chunying Wang,[2] Limei Zheng,[2] Bin Yang,[2] and Wenwu Cao[2,3,†]
[1]*School of Civil Engineering, Harbin Institute of Technology, Harbin, 150001, China*
[2]*Condensed Matter Science and Technology Institute, Harbin Institute of Technology, Harbin, 150080, China*
[3]*Department of Mathematics and Materials Research Institute, The Pennsylvania State University, University Park, Pennsylvania 16802, USA*

(Received 7 December 2017; published 28 February 2018)

Landau free-energy expansion parameters for $0.64Pb(Mg_{1/3}Nb_{2/3})O_3$-$0.36PbTiO_3$ single crystal were determined from the temperature-dependent polarization-electric field (P-E) hysteresis loops along $[001]_C$, the temperature-dependent dielectric constant ε_{11}, and the electric-field-induced tetragonal-rhombohedral phase-transition temperature. Using these obtained parameters, the phase-transition behavior, polarization, dielectric, and piezoelectric constants can all be calculated, which showed good agreement with experimental results. An orthorhombic-to-tetragonal phase transition was predicted to be around $-15\,^{\circ}$C, near which coexisting orthorhombic phase and tetragonal phase were confirmed by experiments. Based on our calculations, we concluded that the commonly observed monoclinic phase around the orthorhombic-to-tetragonal phase-transition temperature was an adaptive structure due to the coexistence of tetragonal and orthorhombic phases. Additionally, large shear piezoelectric responses exist near room temperature due to the instability caused by the competition between the coexisting tetragonal and orthorhombic phases.

DOI: 10.1103/PhysRevB.97.054114

I. INTRODUCTION

Relaxor-based ferroelectric single crystals $(1-x)Pb(Mg_{1/3}Nb_{2/3})O_3$-$xPbTiO_3$ (PMN-xPT) have extraordinary large piezoelectric and dielectric properties and have been extensively studied over the past two decades [1–3]. Those functional properties were greatly enhanced near the morphotropic phase boundary (MPB), which was attributed to the bridging monoclinic (M) phases and the easy rotation between the rhombohedral (R) and tetragonal (T) phases [4–9]. Recently, PMN-xPT with high PT compositions has attracted a great deal of interest for their stable properties in a wider temperature range [10–12]. With domain engineering, the single crystal with ordered-T-phase structures shows a large piezoelectric response and high electromechanical coupling factors [13,14]. For better understanding the physical origin and precise control of the engineered-T-phase structures in relaxor-based ferroelectrics, quantitative theoretical interpretations are highly desired.

Recently, the Landau coefficients of six-order Landau-Devonshire-type free-energy expansion for the R-phase $0.70Pb(Mg_{1/3}Nb_{2/3})O_3$-$0.30PbTiO_3$ were experimentally measured [15]. Using those obtained parameters, ferroelectric and dielectric properties were quantitatively calculated, which agreed well with experimental results in the ferroelectric state. In order to understand the mystery behind the giant piezoelectric properties and correlate them with domain patterns in PMN-PT single crystals, we need to get the Landau parameters for other compositions. The Landau parameters along the $[001]_C$ direction of the single crystals with pure tetragonal phase are relatively easy to be determined, but parameters in other directions are hard to be extracted since the tetragonal phase is rather stable, and other phases could not be easily induced by external electric field. Furthermore, single crystals with high PT compositions are easy to break under large electric field, which adds more difficulties during the poling process. In the following, we use single-crystal $0.64Pb(Mg_{1/3}Nb_{2/3})O_3$-$0.36PbTiO_3$ (PMN-0.36PT), which has the composition near the MPB but in the tetragonal phase, and is relatively easy to facility the electric-field-induced phase transition [16,17].

II. EXPERIMENTAL PROCEDURE

The PMN-0.36PT single crystals were grown by the modified Bridgeman method and oriented by the Laue x-ray machine. The PT content was determined by comparing the Curie temperature with the phase diagram given by synchrotron x-ray powder diffraction [16]. To avoid oxygen defects, all samples were annealed at $600\,^{\circ}$C for 1 h before further processing. Two kinds of plates were prepared for extracting the Landau parameters. One (sample No. 1) was cut into a 4-mm//$[100]_C$ × 4-mm//$[010]_C$ × 0.5-mm//$[001]_C$ plate with gold electrodes sputtered onto the $(001)_C$ and $(00\bar{1})_C$ faces for the measurements of P-E loops and the dielectric constant ε_{33} along $[001]_C$. Another one (sample No. 2) was cut into a 3-mm//$[100]_C$ × 4-mm//$[010]_C$ × 0.5-mm//$[001]_C$ plate for measuring the dielectric constant ε_{11}.

Sample No. 1 was heated at a rate of $3\,^{\circ}$C/min from room temperature to $175\,^{\circ}$C and poled under an electrical field of 15 kV/cm for 20 min at $175\,^{\circ}$C. Then, the crystals were cooled down to room temperature at a rate of $5\,^{\circ}$C/min with the

*luxy@hit.edu.cn
†dzk@psu.edu

electric field on. At room temperature, the electric field was removed at a rate of 0.5 kV/cm per min. Dielectric properties were measured from −100 to 330 °C using an LCR meter (Agilent, E4980A) with the heating rate of 2 °C/min at the frequencies of 1, 10, and 100 kHz. After the measurement of dielectric constants in the heating process, the crystal was put into a silicon oil bath for the measurement of P-E loops using the Precision Premier II system (Radiant Tech., USA). The loops were measured along $[001]_C$ using an ac field of 0.1 Hz with the field magnitude of 10 kV/cm. To fully record the behavior near the phase-transition temperature, the temperature increasing step was set at 1 °C around the tetragonal-to-cubic phase-transition temperature of 169 °C, i.e., from 160 to 180 °C, and 5 °C from room temperature to 160 °C. All data were recorded after the temperature in the oil bath became stable. Since single-domain state is required for extracting the Landau parameters, polarizing light microscopy (Zeiss Axioskop 40) with crossed polarizer/analyzer pairs was used to verify the domain configurations; the results are provided in the Appendix.

To measure the dielectric constant ε_{11}, sample No. 2 was poled along $[001]_C$ under the electric field of 10 kV/cm at 175 °C for 20 min, then cooled down to room temperature at the rate of 5 °C/min. After poling, silver paste electrodes were removed using acetone, then the $(001)_C$ and $(00\bar{1})_C$ surfaces were sputtered with gold electrodes. The dielectric constant ε_{11} was measured from 30 to 170 °C using an LCR meter (Agilent, E4980A) with the heating rate of 2 °C/min at the frequency of 1 kHz.

The temperature-dependent dielectric constants ε_{33} and spontaneous polarization P_3 are shown in Fig. 1. The spontaneous polarization was extracted from the P-E loops during the heating process as an extension from the saturated polarization (inset of Fig. 1). The temperature-dependent dielectric constants ε_{33} at frequencies of 1, 10, and 100 kHz were measured during the heating procedure. The dielectric constant is almost frequency independent below 169 °C and shows only slightly diffused characteristic after the $T \rightarrow C$ phase transition. According to the dielectric curve, there are three temperature regions corresponding to different polarization states. At the temperature range of −10 to 169 °C, the crystal is in the tetragonal state with a typical hysteresis loop similar to the inset of Fig. 1 at 70 °C. The existence of the tetragonal phase in a large temperature range can further simplify the Landau parameters along $[001]_C$. At a lower temperature around −10 °C, another dielectric peak appears which indicates a sharp phase transition.

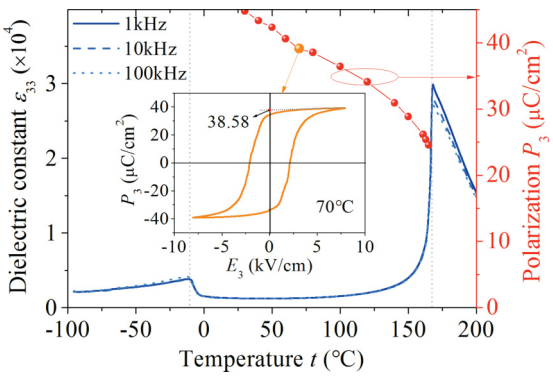

FIG. 1. Temperature-dependent polarization and dielectric constant at frequencies of 1, 10, and 100 kHz. The insert is a typical tetragonal P-E loop at 70 °C.

III. FITTINGS OF EXPERIMENTAL RESULTS

Landau free energy up to six-order expansions was adopted to describe the ferroelectric behavior in the relaxor-based ferroelectric single crystal [15]. Under an external field of arbitrary direction, the Landau-Devonshire free energy with stress X_i and polarization P_i as the order parameters can be expressed as

$$\begin{aligned} G = {} & \alpha_1\left(P_1^2+P_2^2+P_3^2\right)+\alpha_{11}\left(P_1^4+P_2^4+P_3^4\right) \\ & +\alpha_{12}\left(P_1^2P_2^2+P_2^2P_3^2+P_3^2P_1^2\right) \\ & +\alpha_{111}\left(P_1^6+P_2^6+P_3^6\right)+\alpha_{112}\left[P_1^2\left(P_2^4+P_3^4\right)\right. \\ & \left.+P_2^2\left(P_3^4+P_1^4\right)+P_3^2\left(P_1^4+P_2^4\right)\right]+\alpha_{123}P_1^2P_2^2P_3^2 \\ & -\tfrac{1}{2}s_{11}\left(X_1^2+X_2^2+X_3^2\right)-s_{12}\left(X_1X_2+X_2X_3\right. \\ & \left.+X_3X_1\right)-\tfrac{1}{2}s_{44}\left(X_4^2+X_5^2+X_6^2\right) \\ & -Q_{11}\left(X_1P_1^2+X_2P_2^2+X_3P_3^2\right)-Q_{12}\left[X_1\left(P_2^2+P_3^2\right)\right. \\ & \left.+X_2\left(P_3^2+P_1^2\right)+X_3\left(P_1^2+P_2^2\right)\right] \\ & -Q_{44}\left(X_4P_2P_3+X_5P_1P_3+X_6P_2P_1\right) \\ & -E_1P_1-E_2P_2-E_3P_3, \end{aligned} \tag{1}$$

where α_1, α_{11}, α_{12}, α_{111}, α_{112}, and α_{123} are the linear and nonlinear dielectric stiffness coefficients; s_{ij} and Q_{ij} are the elastic compliances and electrostrictive coefficients, respectively.

A. Double-hysteresis loops along $[001]_C$

During the heating process, P-E loops measured below the $T \rightarrow C$ phase-transition temperature are typical single-hysteresis loops, similar as the one inset in Fig. 1 at 70 °C. When the temperature approached the $T \rightarrow C$ phase-transition temperature t_C, double loops were observed as shown in Fig. 2. The double loop was initially observed at $t_1 = 169$ °C, at which the field-induced cubic-to-tetragonal phase transition occurred [18]. For the tetragonal phase, the free energy can be simplified as a function of the polarization component P_3 along the field direction x_3 in the Cartesian coordinate system:

$$G_{001} = \alpha_1 P_3^2 + \alpha_{11} P_3^4 + \alpha_{111} P_3^6 - E_3 P_3. \tag{2}$$

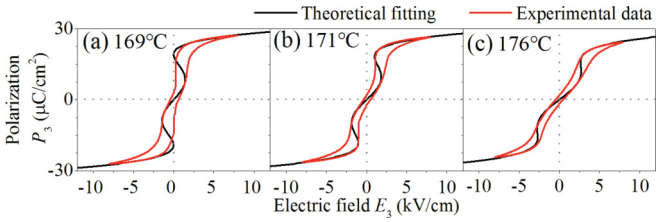

FIG. 2. Theoretical fittings of $[001]_C$-oriented PMN-0.36PT hysteresis loops at (a) 169 °C, (b) 171 °C, and (c)176 °C.

TABLE I. Parameters obtained from the $[001]_C$ hysteresis loops.

t(°C)	α_1 (10^6 m/F)	α_{11} (10^8 m^5/C^{2}F)	α_{111} (10^9 m^9/C^{4}F)
169	1.3110	−0.3575	0.3250
171	1.5120	−0.3550	0.3233
176	1.9980	−0.3475	0.3235

From Eq. (2) we can derive the relationship between the applied electric field E_3 and the polarization P_3 along $[001]_C$ to be

$$E_3 = 2\alpha_1 P_3 + 4\alpha_{11} P_3^3 + 6\alpha_{111} P_3^5. \quad (3)$$

The nonlinear behavior of the polarization under an electric field is controlled by the nonlinear terms $\alpha_{11} P_3^3$ and $\alpha_{111} P_3^5$, especially near the paraelectric-to-ferroelectric phase-transition temperature. Therefore, the Landau expansion coefficients can be extracted by fitting the measured double-hysteresis loops. In fitting the double loops, we have given more weighting to the dominating characters, such as the polarization at high electric field and the coercive field. The obtained expansion coefficients at different temperatures are listed in Table I.

In this case, the parameter α_1 is linearly dependent on temperature t, $\alpha_1 = 0.795 \times 10^5 (t - 152.5)$ (m/F). The Curie constant is $C = 7.107 \times 10^5$ °C, which is usually on the order of 10^5 for displacive ferroelectrics (1.5×10^5 °C for $PbTiO_3$) [19]. We should note that α_1 cannot be obtained by fitting the Curie-Weiss law above the Curie temperature due to the relaxor nature above t_c. α_{11} is slightly temperature-dependent and can be expressed as $\alpha_{11} = 1.489 \times 10^5 (t - 409.2)$ (m^5/C^{2}F); α_{111} is almost temperature-independent and determined to be 0.324×10^9(m^9/C^{4}F). A key cross-check feature is that the double-hysteresis loop begins to separate at a particular $t_1 = 169$ °C, and the parameters must obey the relationship $3\alpha_1\alpha_{111} = \alpha_{11}^2$ [20]. Our results show high accordance with these requirements.

B. Dielectric constant ε_{11}

An effective way to obtain parameters α_{12} and α_{112} is to fit the spectrum of temperature-dependent dielectric constant ε_{11} in the tetragonal phase with polarization along $[100]_C$, which can be derived from the relationship $\varepsilon_{11} = \partial P_1/\partial E_1 = [(2\alpha_1 + 2\alpha_{12} P_3^2 + 2\alpha_{112} P_3^4)\varepsilon_0]^{-1}$ [21]. With the obtained parameter α_1 and the polarization in the tetragonal phase, the measured ε_{11} of the crystal from 30 to 165 °C can be fitted by using the least-squares method as shown in Fig. 3, where we extracted the temperature-independent parameters $\alpha_{12} = 6.60 \times 10^7$m^5/C^{2}F and $\alpha_{112} = 1.05 \times 10^8$m^9/C^{4}F.

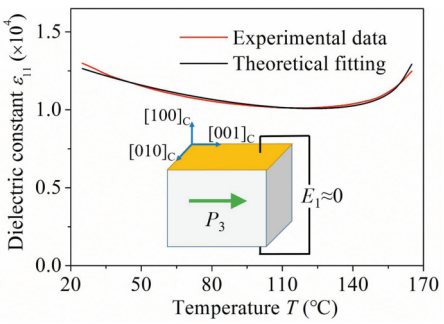

FIG. 3. Theoretical fitting of dielectric constant ε_{11}. The inset is the schematic of the measurement configuration.

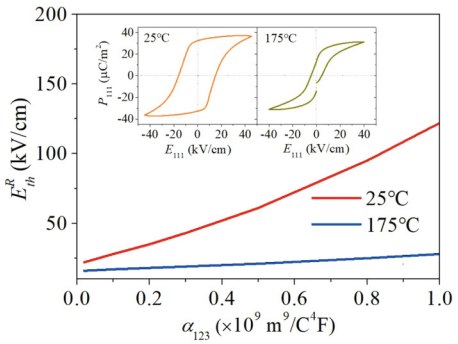

FIG. 4. Relationship between the parameter α_{123} and the threshold electric field of the formation of R phase.

C. Existence of the R phase and the parameter α_{123}

To obtain the parameter α_{123}, the R phase is preferred. Unfortunately, there is no pure R phase for the PMN-0.36PT single crystal in the whole temperature range. An alternative method is to probe the threshold of the electric field E_{th}^R along $[111]_C$ with respect to the α_{123}. To do this, we first gave a value of α_{123} on the order of 10^9. Together with the obtained other parameters, i.e., α_1, α_{11}, α_{12}, α_{111} and α_{112}, we could calculate the phase transition from T to R under an electric field along the $[111]_C$ direction, where the threshold electric field E_{th}^R for the T-R phase transition can be obtained with each given value of α_{123} at a particular temperature by minimizing the free energy. As shown in Fig. 4, the E_{th}^R is very sensitive to the parameter α_{123} at 25 °C and insensitive at high temperatures. With the fact that there is no obvious T to R phase transition at 25 °C even with an applied electric field as high as 50 kV/cm (hysteresis loop as inset in Fig. 4), we could conclude that $\alpha_{123} > 0.4 \times 10^9$ m^9/C^{4}F. At high temperature, such as 175 °C, E_{th}^R is almost a constant around 20 kV/cm. In other words, the R phase could be induced by applied electric field above 20 kV/cm. Under an electric field of 40 kV/cm at 175 °C, the polarization was believed to switch to $[111]_C$ with a saturation value of about 31.32 μC/m^2 as shown in the inset of Fig. 4. Using the formula of $E_{111} = 2\alpha_1 P_{111} + 4\alpha_{11}^R P_{111}^3 + 6\alpha_{111}^R P_{111}^5$ with $\alpha_{11}^R = \frac{1}{3}(\alpha_{11} + \alpha_{12})$, and $\alpha_{111}^R = \frac{1}{27}(3\alpha_{111} + 6\alpha_{112} + \alpha_{123})$, we were able to obtain the parameter α_{123} to be 0.790×10^9 m^9/C^{4}F. We should note that the theoretical coercive field is close to the experimental one at high temperatures, although it is always higher than the experimental one at room temperature or lower temperatures due to the domain wall mediated switching behaviors in experiments.

IV. VERIFICATION OF PREDICTED RESULTS BY EXPERIMENTS

Up to this point, we have obtained the sixth-order Landau-Devonshire expansion parameters for the PMN-0.36PT single crystal. Together with the elastic constants s_{ij} and

TABLE II. Landau parameters, elastic constants s_{ij}, and electrostrictive constants Q_{ij} of the PMN-0.36PT single crystal.

Parameters of PMN-0.36PT			
t_0(°C)	152.5 °C	Q_{11}(m^4/C^2)	0.050
C (10^5 °C)	7.107	Q_{12}(m^4/C^2)	− 0.0245
α_0(10^5m/F °C)	0.795	Q_{44}(m^4/C^2)	0.018
α_1(10^5m/F)	0.795 × (t−152.5 °C)	s_{11}($10^{-12}m^2$/N)	9.75
α_{11}($10^5m^5/C^2F$)	1.489 × (t−409.2 °C)	s_{12}($10^{-12}m^2$/N)	− 2.56
α_{12}($10^8m^5/C^2F$)	0.660	s_{13}($10^{-12}m^2$/N)	− 3.79
α_{111}($10^9m^9/C^4F$)	0.324	s_{33}($10^{-12}m^2$/N)	10.36
α_{112}($10^9m^9/C^4F$)	0.105	s_{44}($10^{-12}m^2$/N)	15.88
α_{123}($10^9m^9/C^4F$)	0.790	s_{66}($10^{-12}m^2$/N)	15.92

electrostrictive constant Q_{ij} for the tetragonal phase (Ref. [12]), all parameters are listed in Table II.

Since the obtained Landau parameters are mainly extracted from high-temperature hysteresis loops and dielectric constant ε_{11}, it is necessary to verify their validity using theoretical predictions on other quantities to compare with experimental results, including spontaneous elastic strains, temperature-dependent polarization, dielectric constants, and piezoelectric constants.

For the tetragonal phase, the spontaneous elastic strains are given by $S_1 = S_2 = Q_{12}\ P_3^2$ and $S_3 = Q_{11}\ P_3^2$ [22]. Thus, the electrostrictive coefficients Q_{ij} can be obtained with the spontaneous polarization and strains. The spontaneous polarization can be written as $P_s^2 = (-\alpha_{11} + \sqrt{\alpha_{11}{}^2 - 3\,\alpha_1\,\alpha_{111}})/3\alpha_{111}$. As shown in Fig. 5(a), the polarization can be well-fitted in a wide range of temperature by using the free energy with parameters obtained in this work. The errors of fittings are less than 1% over the whole temperature range. Using the synchrotron x-ray powder-diffraction results, the strains in the tetragonal phase can be calculated using $S_1 = S_2 = (a_T - a_C')/a_C'$, $S_3 = (c_T - a_C')/a_C'$, where a_T and c_T are the lattice constants of the tetragonal structure; a_C' is the lattice constant of the cubic structure extrapolated into the tetragonal region [23]. The electrostrictive coefficients used here are $Q_{11} = 0.050\,m^4/C^2$ and $Q_{12} = -0.0245\,m^4/C^2$, which are comparable with the values $Q_{11} = 0.056\,m^4/C^2$, and $Q_{12} = -0.024\,m^4/C^2$ given in Ref. [24]. Using these parameters, the spontaneous strains S_1 and S_3 can be well-fitted as shown in Fig. 5(b), which validates the free-energy expansion parameters we have obtained for the tetragonal phase.

To check the validity of these parameters in a broader temperature range, we calculated the stable polarization and verified the phase stability using the Hessian matrix [4,15]. As shown in Fig. 6(a), O and T phases have equal free energy at −15 °C, indicating a possible phase transition around this temperature. Compared with the phase-transition temperature obtained from the dielectric spectrum (Fig. 1) of about −10 °C, it still shows a reasonable agreement with the theoretical prediction. Around the phase-transition temperature, the O and T phases with similar energies can coexist in a wide

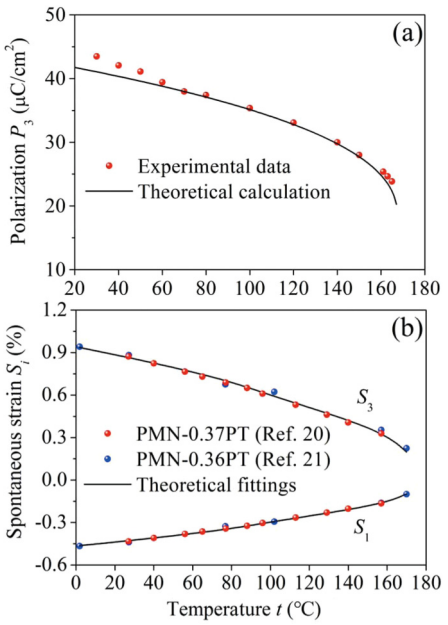

FIG. 5. Theoretical and experimental (a) spontaneous polarization and (b) spontaneous strains vs temperature.

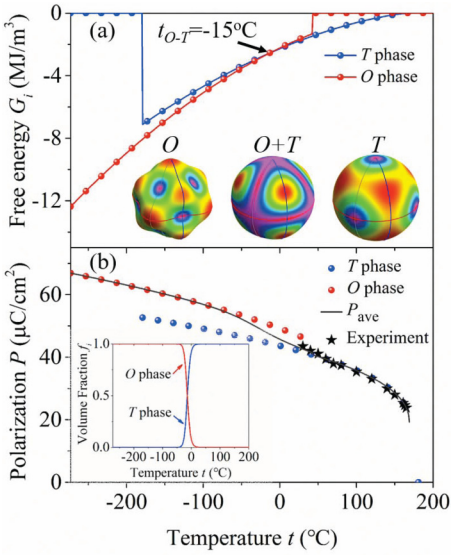

FIG. 6. Calculated temperature-dependent free energies (a) and polarizations (b) of the O and T phases with obtained Landau parameters. Experimental results of polarization were also given for comparison. Insets in (a) are the energy surfaces for dominating O phase, $T + O$ phases, and T phase. The volume fractions of T and O phases around the O-T phase-transition temperature are inset in (b).

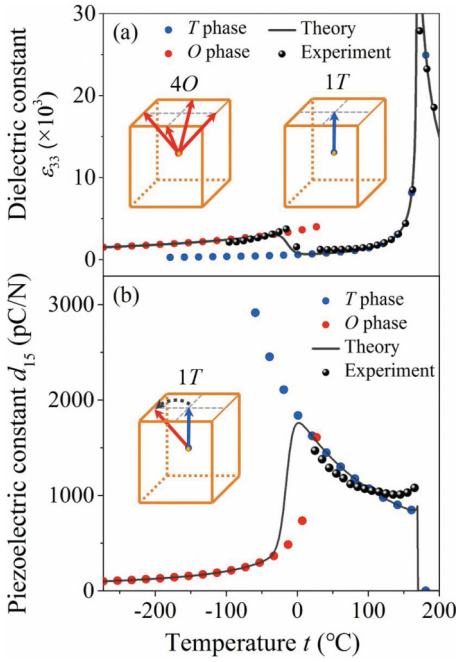

FIG. 7. Comparison of calculated and measured dielectric constant ε_{33} (a) and shear piezoelectric constant d_{15} (b). Insets in (a) are schematics of the $4O$ mulitdomain and $1T$ single domain, respectively.

temperature range [22]. As shown in the energy surfaces [insets in Fig. 6(a)], the T phase dominates above the phase-transition temperature, and coexists with the O phase near the phase-transition temperature. With further decreasing temperature, the dominating T phase becomes unstable and is replaced by the emerging O phase. The corresponding volume fractions $f_i(i = T, O)$ with the domain size of 5000 unit cells can be calculated based on the canonical distribution theory [25] and are shown in the inset of Fig. 6(b). Synchrotron x-ray powder-diffraction results have shown that there is a phase transition from M_C to T during the heating process [16]. Since O and T phases can be easily distorted in the coexistence region, it is possible that the M_C phase observed in the synchrotron x-ray powder diffraction is a distorted O or T phase as an adaptive structure at the interface of coexisting phases [26,27].

To further verify the obtained expansion parameters and the phase-coexisting hypothesis, we calculated the dielectric constant and shear piezoelectric constant separately in each phase. In order to compare them with experimental results, we calculated the average values by using the volume fractions of each phase [26]. As shown in Fig. 7(a), the calculated dielectric constants in both the O and T phases coincide well with experimental values. The $[001]_C$ poled PMN-0.36PT single crystal at temperatures lower than $-15\,^{\circ}$C is mostly in the $4O$ multidomain state, possibly coexisting with a small amount of T phase and O-like M_C phase. The dielectric constant ε_{33} of the $4O$ state along $[001]_C$ is equal to that of the $1O$ state along $[001]_C$, thus the theoretical calculations can be directly compared with experimental results. Slight discrepancy exists near the O-T phase-transition temperature where several phases coexist. The adaptive strain can make the crystal structure distorted in a complex way, which may enhance the dielectric response due to the monocliniclike phases with lower symmetry. Specifically, the crystal may exhibit high shear piezoelectricity due to the existence of T-to-O phase transition, which is suitable for shear electromechanical transducers [14]. The shear piezoelectricity was calculated and compared with experimental results. As shown in Fig. 7(b), the shear piezoelectric constant d_{15} has a large increase near the O-T phase-transition temperature, indicating that the tetragonal phase begins to lose the crystallographic stability and coexists with the orthorhombic phase. At even lower temperature, orthorhombic phase eventually dominates, corresponding with a low d_{15}. We should note that the temperature range where two phases can coexist is dependent on the domain size as described before.

V. SUMMARY

In this work, we have determined the sixth-order Landau-Devonshire expansion parameters for the PMN-0.36PT single crystal. The temperature-dependent polarization, spontaneous strains, and dielectric properties were calculated using these parameters, and show good agreements with experiments, providing convincing validation for these obtained parameters. A phase transition from orthorhombic-to-tetragonal phase was predicted to be around $-15\,^{\circ}$C based on the theory. From energy calculations, the orthorhombic and tetragonal phases can coexist in a small temperature range. We therefore believe that the commonly observed Mc phase may be an adaptive phase due to the interface mismatch between the coexisting orthorhombic and tetragonal phases. In addition, the temperature-dependent shear piezoelectric constant d_{15} has been calculated, which shows a large value of $d_{15} = 1500$ pC/N close to room temperature, indicating the potential for shear transducer applications. These parameters we have obtained make it possible to quantitatively study domain formation and domain dynamics using Landau-like models; they will facilitate the theoretical study to understand the origin of the ultrahigh piezoelectric properties in these domain-engineered PMN-xPT single crystals.

ACKNOWLEDGMENTS

This research was supported by the National Natural Science Foundation of China (Grants No. 11372002 and No. 51572055), the National Key Basic Research Program of China (Grant No. 2013CB632900), and the PIRS of HIT (Grant No. B201509).

APPENDIX

In order to determine the expansion parameters of the free energy within the framework of the Landau theory, samples are required in the single-domain state, which were verified by using the polarizing light microscopy (PLM) based on the birefringence of crystals. To observe the domain structure under certain temperature or applied electric field, we used PLM (Zeiss Axioskop 40) equipped with a heating-cooling optical stage (Linkam THMS400) and a dc source with a dc bias fixture (Agilent 16065A).

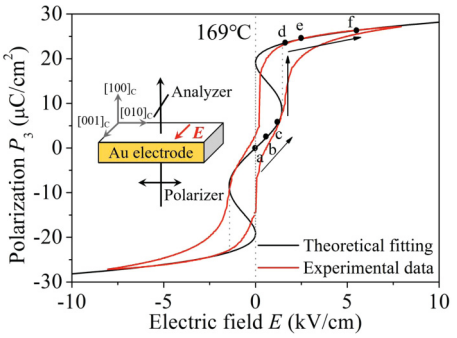

FIG. 8. P-E hysteresis loop under an electric field along $[001]_C$ at 169 °C. Inset is the illustration of the sample with applied crossed analyzer/polarizer pairs and the applied electric field.

1. Double-hysteresis loops at 169 °C under electric field along $[001]_C$

Both experiments and Landau theory show that a special double loop exists at a particular temperature t_1 under an electric field (Fig. 8). To probe the phase change under electric fields and verify the single-domain state of $[001]_C$ poled crystal at this temperature, a thin and slim plate (sample No. 3) was prepared with dimensions of $1.0\,\text{mm}//[001]_C \times 3.0\,\text{mm}//[010]_C \times 0.7\,\text{mm}//[100]_C$. The $(001)_C$ surfaces were fine polished for domain observations. Before the measurement, the sample was annealed at 350 °C for 1 h to eliminate the stresses induced by cutting and polishing. Gold films were vacuum sputtered onto the $(001)_C$ and $(00\bar{1})_C$ surfaces as electrodes. The temperature was increased from room temperature to 169 °C (above t_C) at a step of 5 °C and then kept at 169 °C. The angle between the polarizer and the [010] direction was defined as θ. As shown in Fig. 9,

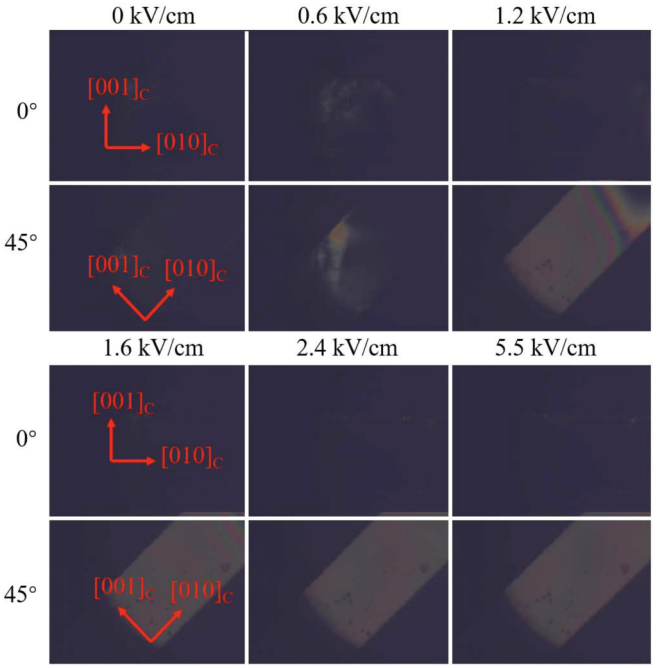

FIG. 9. Electric-field-dependent phase changes at 169 °C with a dc electric field applied along $[001]_C$ observed at the polarizer angle of 0 and 45°, respectively.

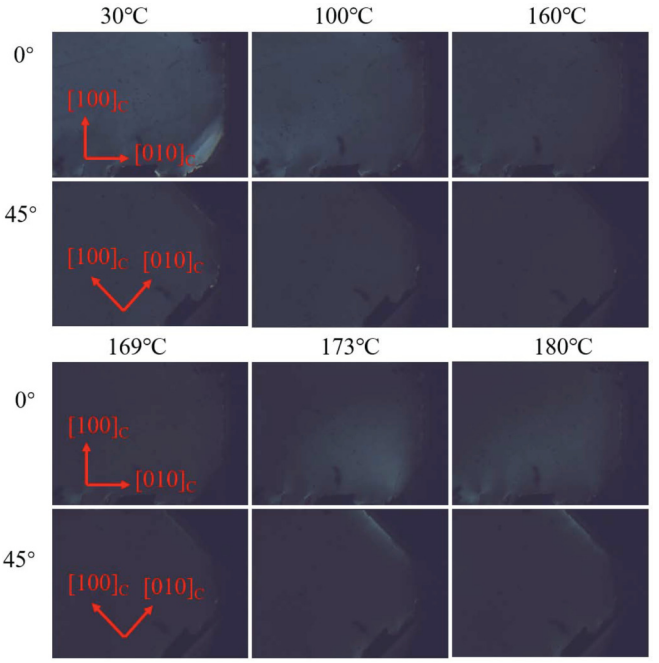

FIG. 10. PLM results for the heating procedure from 30 to 180 °C with single-domain state observed at the polarizer angle of 0 and 45°, respectively.

light is completely extinct in both θ angles of 0 and 45° at zero field, indicating the cubic phase. We should note that polar nano-regions (PNRs)s cannot be visualized by PLM at high temperatures because they are too small for the optical microscopy resolution. When the applied electric field was increased from zero to 0.6 kV/cm by a small step of 0.1 kV/cm, tetragonal phase began to form both in the in-plane and out-of-plane directions. With further increase of the electric field, the out-of-plane polarization began to shift to the $[001]_C$ direction. When the electric field reached 1.6 kV/cm, the light intensity was the maximum, indicating the complete switching of the tetragonal polarization to the $[001]_C$ direction. Such field-induced transition is rather sharp with collective switching behavior. Further increase of the electric field to 2.4 or 5.5 kV/cm does not change the domain structure too much. We note that this tetragonal phase can only be kept under high electric fields.

2. Single-domain T phase in the temperature range of 30 to 170 °C

To confirm the single-domain tetragonal phase in the temperature range of 30 to 169 °C, another thinner plate (sample No. 4) with the dimensions of $0.2\,\text{mm}//[001]_C \times 2.5\,\text{mm}//[010]_C \times 2.5\,\text{mm}//[100]_C$ was prepared. Before the PLM experiments, the sample was poled under an electric field of 10 kV/cm along $[001]_C$ for 20 min at room temperature. As shown in Fig. 10, the extinction patterns both at 0 and 45° showed that the single-domain (c domain) state is stable from 30 to 169 °C.

3. O phase below −15 °C

Based on the dielectric measurements, there is a transition between the lower-temperature O phase and the

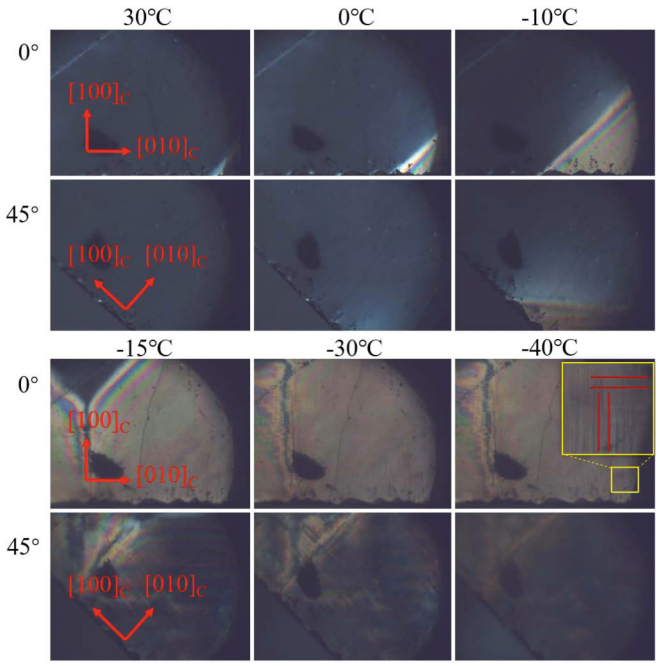

FIG. 11. PLM results for the cooling procedure from 30 to −40 °C with single-domain state observed at the polarizer angle of 0 and 45°, respectively.

higher-temperature T phase. To verify this phase transition, we poled sample No. 4 under the electric field of 10 kV/cm along $[001]_C$ for 20 min at room temperature, then removed the

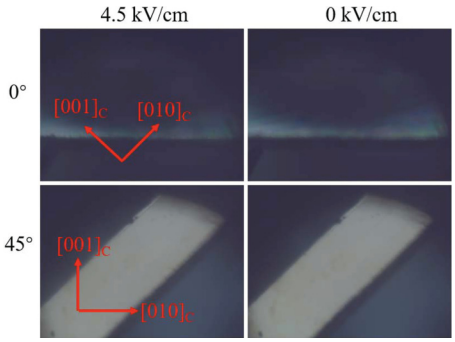

FIG. 12. PLM results with an electric field applied along $[011]_C$ at −30 °C observed at the polarizer angle of 0 and 45°, respectively.

electrodes. As shown in Fig. 11, the stable T phase at 30 °C was kept with the decrease of the temperature until the temperature reached −10°C, where a sudden phase transition exists between −10 and −15 °C with possible O or R phase extinction pattern. Combined with the above theoretical calculation, $4O$ domain state is reasonable with stripe domain walls as shown in the amplifying inset.

To further confirm the stability of the O phase at low temperatures, another plate (sample No. 5) with the dimensions of $0.6\,\text{mm}//[001]_C \times 2.5\,\text{mm}//[110]_C \times 2.5\,\text{mm}//[1\bar{1}0]_C$ was prepared to study the electric-field-dependent phase evolution at −30 °C. Gold film was vacuum sputtered onto the $(110)_C$ and $(\bar{1}10)_C$ surfaces as electrodes. As shown in Fig. 12, the extinction patterns showed that the O phase can be stabilized after the crystal being poled with an electric field of 4.5 kV/cm along $[110]_C$.

[1] S. E. Park and T. R. Shrout, J. Appl. Phys. **82**, 1804 (1997).
[2] E. Sun and W. W. Cao, Prog. Mater. Sci. **65**, 124 (2014).
[3] L. M. Zheng, R. Sahul, S. J. Zhang, W. H. Jiang, S. Y. Shi, and W. W. Cao, J. Appl. Phys. **114**, 104105 (2013).
[4] X. Y. Lu, L. M. Zheng, H. Li, and W. W. Cao, J. Appl. Phys. **117**, 134101 (2015).
[5] D. Damjanovic, Appl. Phys. Lett. **97**, 062906 (2010).
[6] M. Ahart, M. Somayazulu, R. Cohen, P. Ganesh, P. Dera, H. k. Mao, R. J. Hemley, Y. Ren, P. Liermann, and Z. Wu, Nature **451**, 545 (2008).
[7] J. Luo and X. Geng, Prog. Mater. Sci. **68**, 1 (2015).
[8] R. Pirc and R. Blinc, Phys. Rev. B **76**, 020101 (2007).
[9] G. Xu, Z. Zhong, Y. Bing, Z. G. Ye, and G. Shirane, Nat. Mater. **5**, 134 (2006).
[10] F. Li, S. Zhang, Z. Xu, X. Wei, J. Luo, and T. R. Shrout, J. Appl. Phys. **108**, 034106 (2010).
[11] H. Cao, V. H. Schmidt, R. Zhang, W. Cao, and H. Luo, J. Appl. Phys. **96**, 549 (2004).
[12] Y. J. Jing, L. M. Zheng, W. M. Lü, Z. Z. Xi, P. Zheng, J. Du, and R. Zhang, Phys. Status Solidi B **253**, 1994 (2016).
[13] F. Li, S. Zhang, Z. Xu, X. Wei, J. Luo, and T. R. Shrout, J. Am. Ceram. Soc. **93**, 2731 (2010).
[14] L. Zheng, Y. Jing, X. Lu, R. Wang, G. Liu, W. Lü, R. Zhang, and W. Cao, Phys. Rev. B **93**, 094104 (2016).
[15] H. B. Zhang, X. Y. Lu, R. X. Wang, C. Y. Wang, L. M. Zheng, Z. Liu, C. Yang, R. Zhang, B. Yang, and W. W. Cao, Phys. Rev. B **96**, 054109 (2017).
[16] B. Noheda, D. E. Cox, G. Shirane, J. Gao, and Z. G. Ye, Phys. Rev. B **66**, 054104 (2002).
[17] A. K. Singh, D. Pandey, and O. Zaharko, Phys. Rev. B **74**, 024101 (2006).
[18] W. Merz, Phys. Rev. **91**, 513 (1953).
[19] F. Jona and G. Shirane, *Ferroelectric Crystals* (Dover, New York, 1993).
[20] X. Y. Lu, H. Li, and W. W. Cao, J. Appl. Phys. **114**, 224106 (2013).
[21] M. J. Haun, E. Furman, S. J. Jang, H. A. McKinstry, and L. E. Cross, J. Appl. Phys. **62**, 3331 (1987).
[22] O. Noblanc, P. Gaucher, and G. Calvarin, J. Appl. Phys. **79**, 4291 (1996).
[23] A. K. Kalyani, D. K. Khatua, B. Loukya, R. Datta, A. N. Fitch, A. Senyshyn, and R. Ranjan, Phys. Rev. B **91**, 104104 (2015).
[24] F. Li, L. Jin, Z. Xu, D. W. Wang, and S. J. Zhang, Appl. Phys. Lett. **102**, 152910 (2013).
[25] X. Y. Lu, H. B. Zhang, L. M. Zheng, and W. W. Cao, J. Appl. Phys. **122**, 054102 (2017).
[26] X. Y. Lu, H. B. Zhang, L. M. Zheng, and W. W. Cao, AIP Adv. **6**, 105208 (2016).
[27] V. Y. Topolov, Phys. Rev. B **65**, 094207 (2002).